






Capillary discharge in the high repetition rate regime

P. Sasorov ^{1,*}, G. Bagdasarov ¹, N. Bobrova ², G. Grittani,¹ A. Molodzhentsev ¹ and S. V. Bulanov ^{1,3}

¹*ELI Beamlines Facility, Extreme Light infrastructure ERIC, 252 41 Dolni Brezany, Czech Republic*

²*Faculty of Nuclear Sciences and Physical Engineering, Czech Technical University in Prague, Brehova 7, 115 19 Prague, Czech Republic*

³*National Institutes for Quantum and Radiological Science and Technology (QST), Kansai Photon Science Institute, Kizugawa, Kyoto 619-0215, Japan*



(Received 18 May 2023; accepted 15 December 2023; published 18 March 2024)

Plasma discharge in the capillary is used to develop x-ray lasers, waveguides for high power laser pulses, and as active plasma lenses to focus high energy charged particle beams. Capillary discharges in the high repetition rate regime are of interest for applications that require large average values, such as luminosity and/or electric current of laser accelerated particles. In the present paper, we study the capillary discharge in the high repetition rate regime in connection with the ultrashort laser pulse guiding for laser electron acceleration. Using magnetohydrodynamic computer simulations and theoretical scaling, we investigate the filling of the capillary with the gas, the electric discharge development leading to outflow of the plasma from the capillary, and the recovery of gas distribution after the discharge end. In the next cycle, these processes are repeated. As a result, we found the characteristic cycle time, which determines the upper limit on the repetition rate allowed by the capillary parameters. In the case of the capillary discharges used for acceleration of sub-GeV electron beams, e.g., needed for compact free electron lasers, an upper limit on the repetition rate is approximately equal to 10 kHz.

DOI: [10.1103/PhysRevResearch.6.013290](https://doi.org/10.1103/PhysRevResearch.6.013290)

I. INTRODUCTION

Compact laser-based accelerators of relativistic electrons conceive a broad variety of applications, including compact free electron lasers (FELs) [1–7], Compton sources [8–10], and electron-positron colliders [11,12]. References [13–18] demonstrate electron beam generation with laser wake-field acceleration (LWFA) mechanism [19,20].

Plasma discharges in the capillaries are used in a variety of applications, such as standard sources of VUV radiation [21], x-ray lasers [22,23], waveguides for high power laser pulses [17,18,24], and as active plasma lenses [25,26] to focus high energy charged particle beams. In particular, capillary discharges provide electron density distribution, which is suitable for guiding laser pulse drivers, used in the LWFA scheme [17,18,24,27–31]. The capillary discharges for different applications were discussed in detail in Refs. [17,18,24–38].

Capillary discharges in the high repetition rate regime are of interest for different applications. For example, a high repetition rate ($\gtrsim 1$ kHz) of the electron accelerator operation is required [9]. A hydrogen-filled capillary discharge waveguide for LWFA, operating at kHz repetition rates, is considered in Ref. [39]. Other plasma waveguides for LWFA operating

at high repetition rates are described in Refs. [40,41]. Such plasma channels can be used to obtain multi-GeV electron beams [17,18,42].

In this paper, we present the results of simulations and theoretical investigations of the high repetition rate capillary discharge operation and its dependence on the parameters. We consider the following stages of a cycle: filling of the capillary by a cold gas, dynamics of the discharge from its ignition till almost complete recombination of the plasma, and expansion of the gas-plasma into the vacuum region and the gas supplying slots. We also take into account driver laser pulse energy deposition into capillary plasma. We neglect the effects of the processes outside the capillary discharge, leading to potential limitation to the repetition rate of capillary discharge, considered in Ref. [39]. As a result, we find the characteristic cycle time, which determines the upper limit on the repetition rate allowed by the capillary parameters.

We use the code MARPLE [43] for simulations.

II. SIMULATION SETUP

Simulations of the capillary discharge, operating in a repetitive regime, are performed by use of the three-dimensional magnetohydrodynamic (MHD) code MARPLE. It implements two-temperature (ion and electron) MHD equations. It also takes into account the electron and ion thermal conductions, viscosity, and finite electric resistance. The physical model is described in Refs. [38,43–45]. This code has been used in simulations connected with various experiments [18,38,46–48].

*pavel.sasorov@eli-beams.eu

Published by the American Physical Society under the terms of the [Creative Commons Attribution 4.0 International](https://creativecommons.org/licenses/by/4.0/) license. Further distribution of this work must maintain attribution to the author(s) and the published article's title, journal citation, and DOI.

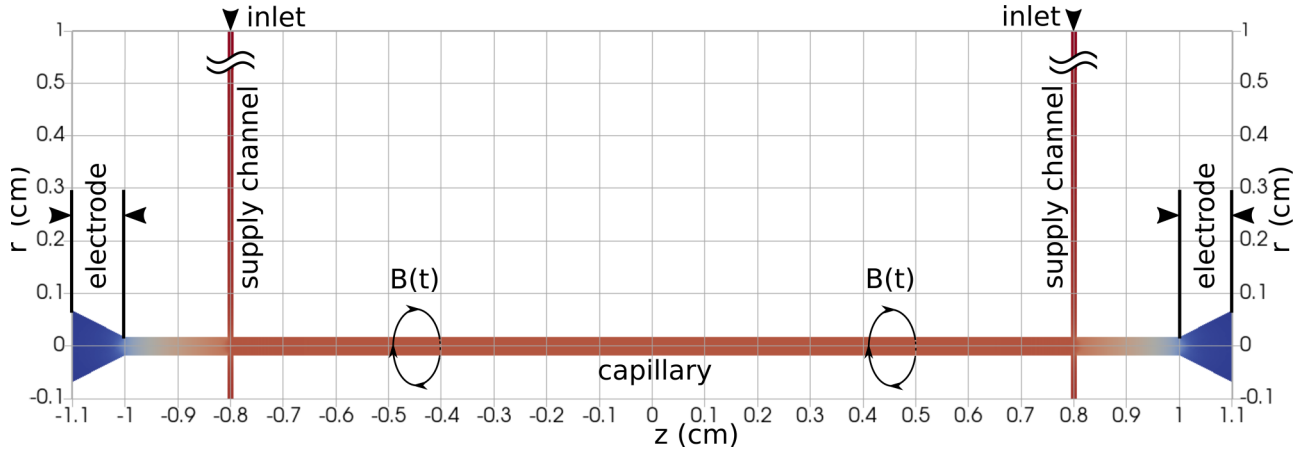


FIG. 1. Overall geometry of the simulation domain. It is azimuthally symmetric. It consists of (i) the capillary of $D = 0.34$ mm diameter and $L = 2$ cm length within the region, $|z| \leq 1$ cm, with ideal rigid dielectric wall; (ii) conical orifices in ideal metal electrodes at 1.1 cm $\leq |z| < 1$ cm; and (iii) two disklike supply channels in ideal rigid dielectric with inlets at $r = 1$ cm.

A full cycle of operation of the capillary discharge in the repetitive regime consists of two phases. One corresponds to the phase of the electric discharge, whereas the second one corresponds to dynamics of neutral hydrogen H_2 gas between the discharges. The cyclic operation of the capillary discharge starts from a process of filling the capillary with the gas. Both phases are simulated with the same code. However, simulation of the electromagnetic field as well as simulation of the electron component of the plasma are switched off during the phases of neutral hydrogen dynamics simulations. The phase of the discharge is simulated with the full MHD code described briefly above.

We assume a circular cross-section shape capillary of length $L = 2$ cm and diameter $D = 2r_0 = 340 \mu\text{m}$. The computational domain is shown in Fig. 1. It includes two supply channels of the width $D/3$ at $|z| = 0.8$ cm as well as the electrode regions (1 cm $< |z| < 1.1$ cm). They play a significant role in the gas and plasma dynamics inside the capillary [45,46]. We assume the length of the simulated part of the supply channels to be equal to 1 cm because the rest of the supply channel plays negligible role in the consequent processes of recovering of the predischARGE gas density distribution.

The considered configuration is azimuthally symmetric. It means, in particular, that the supply channels have a disk shape. We assume that the capillary is made of an ideal absolutely rigid dielectric, whereas the electrodes are made of ideal absolutely rigid metals. These assumptions allow us to set the boundary conditions on the discharge stage. Boundary conditions at $|z| = 1.1$ cm provide free outflow of the gas or plasma. The boundary conditions correspond to the vacuum region outside the capillary, where gas continuously flows from the capillary. The gas outflow is balanced, on average, by the gas inflow provided by the supply channels. The temperature of the capillary and the temperature of electrodes are equal to a room temperature. Simulating the discharge dynamics, we assume the capillary wall and electrode temperature is of 0.5 eV, which is much lower than the typical temperature of the discharge plasma.

The simulation is divided into three stages: stages 1, 2, and 3. Stage 1 models the process of the capillary filling

with a molecular hydrogen gas before the discharge is ignited. The hydrogen gas at the pressure $p = 75$ mbar and at room temperature fills the capillary through the supply channels (inlets marked in Fig. 1). The gas pressure is chosen to achieve the electron density required for LWFA. The final almost steady-state flow obtained at stage 1 (at $t = t_{12} = 200 \mu\text{s}$) is used as an initial condition for the capillary discharge MHD simulations (stage 2). The discharge current has the following form:

$$I(t > t_{12}) = I_0 \frac{t - t_{12}}{t_c} \exp\left(1 - \frac{t - t_{12}}{t_c}\right), \quad (1)$$

where $I_0 = 200$ A and $t_c = 150$ ns. Its profile is shown in Fig. 2. The detailed form of the current pulse is not important for the considered problem. The main parameters of the electric current pulse are peak current, I_0 , and its typical duration (FWHM), that is, $\approx 2.45t_c \approx 370$ ns. The latter parameters are typical for the LWFA experiments [17,18,39]. The azimuthal component of magnetic field at the insulator boundary is $B_\phi = 2I(t)/(cR)$, where $I(t)$ is given by Eq. (1) and R is the

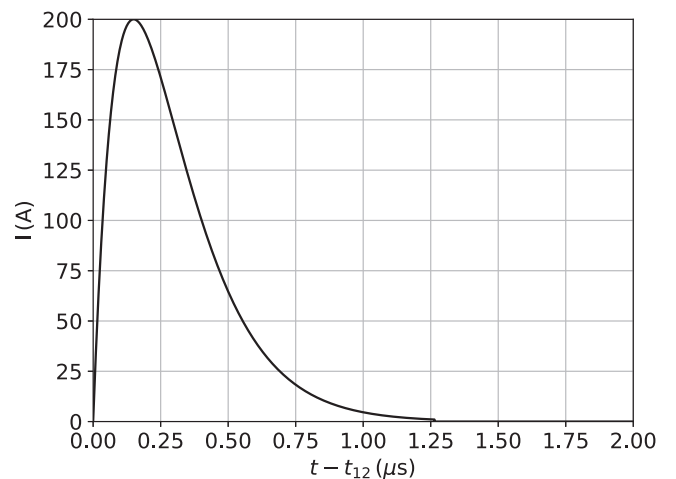


FIG. 2. Total electric current through the capillary discharge vs time during stage 2.

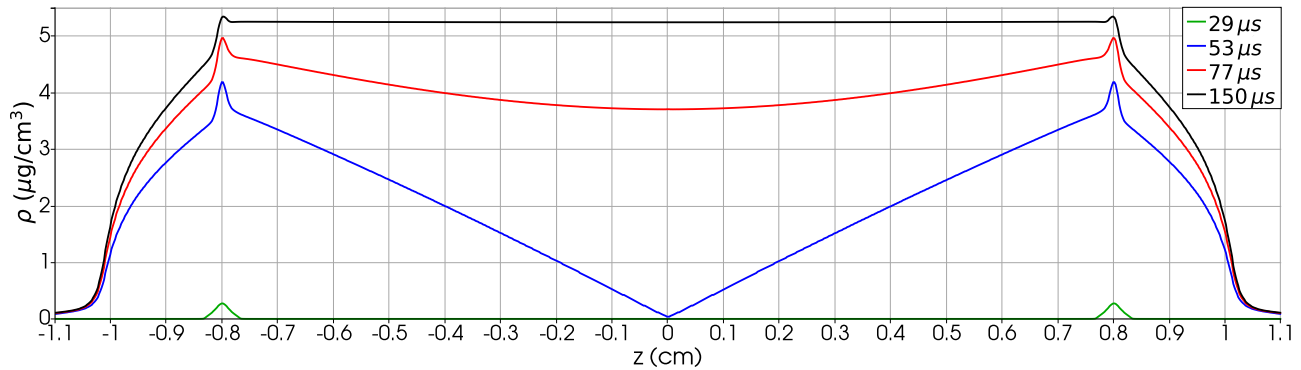


FIG. 3. Gas density distribution during stage 1. 1D density distributions on the axis of the capillary for different time moments are shown. The curves are labeled by the time t .

current radius at the boundary of the computational domain. This determines the boundary condition for the magnetic field. At $t = t_{23} = t_{12} + 2 \mu\text{s} = 202 \mu\text{s}$, when the discharge is ended and plasma is cooled down, stage 2 is finished. Stage 3 models the process of recovering the neutral hydrogen distribution in the capillary, though some capillary refilling begins by the end of stage 2. The final state of stage 2 (at $t = t_{23}$) is used as the initial condition for stage 3. When the steady-state density distribution is reached, stage 3 ends at $t - t_{23} \sim 100\text{--}150 \mu\text{s}$. Thus, the transition between stages 1 and 2 takes place at $t = t_{12} = 200 \mu\text{s}$, and the transition between stages 2 and 3 occurs at $t = t_{23} = 202 \mu\text{s}$.

The physical model implemented in the code MARPLE, presented above, describes evolution of gas (for stages 1 and 3) or plasma (for stage 2) density, ρ , measured in unit mass per unit volume, electron density, n_e , which is the number of electrons per unit volume, electron and ion temperatures, T_e and T_i , and radial and axial velocities, v_r and v_z inside the computational domain. The model also describes the evolution of the azimuthal component of the magnetic field, B_φ . For stages 1 and 3, we exclude the magnetic field, B_φ , and electron temperature, T_e , from the system equations used in the physical model and set $T = T_i$. All above-mentioned values depend (in the azimuthally symmetric case) on r , z , and t , where r is radial coordinate of the cylindrical coordinate system, (r, φ, z) , associated with the capillary axis.

All main parameters of the three-stage simulation, a , L , electron density on the axis $n_e = 2 \times 10^{18} \text{ cm}^{-3}$, energy of the driver femtosecond laser pulse, 3 J, correspond to Ref. [6]. Below we consider the set of these parameters as nominal.

The same discretization of the computational domain is used in all simulation stages. A spatial step of $h_r = 5 \mu\text{m}$ is used along the capillary radius and in the most interesting regions of the computational domain in the z direction, e.g., the junction of supply channel and capillary. The total amount of computational cells of 474 K is partitioned into 112 pieces and processed in parallel.

In Ref. [45], three-dimensional simulation of initial gas filling and discharge in a relatively short square capillary discharge including supply channels, electrodes, and a vacuum external region was presented. Due to the short capillary length (1 cm), it was possible to investigate electric current and plasma density inhomogeneities near the connections of the supply channels with the capillary. 3D simulations of

longer capillaries as considered in Ref. [46] is impossible to carry out in a reasonable computation time.

To achieve the parameters of Ref. [6], we need longer capillaries and to extend the discharge simulation up to much longer time after the beginning of the electric current pulse. To investigate plasma dynamics of such capillary discharges in a repetitive regime, much longer simulations (about 20 times longer) than in Ref. [45] are required. In the considered case, an exact three-dimensional structure of the capillary in the vicinity of its open ends as well as outlets of the supply channels does not affect strongly overall plasma dynamics in the repetitive regime. So, we simplify the problem by introducing the azimuthal symmetry, which allows us to keep the simulation time in a reasonable range. Such simplification will not affect physical processes governing the repetition regime and the evaluation of the allowable repetition rate.

III. RESULTS OF THE SIMULATION

A. Stage 1: Simulation of capillary filling

The main goal of this stage is to obtain a spatial distribution of the gas at the end of the process of capillary filling when a steady state gas flow is established. The evolution of the gas density distribution is shown in Fig. 3. Figure 4 shows gas-plasma density time evolution at the center of the capillary at $r = 0$, $z = 0$ for all three stages of the simulation. The time interval $0 < t < t_{12} = 200 \mu\text{s}$ corresponds to stage 1. Due to the thermal conductivity, the gas temperature is almost equal to the capillary wall temperature, 300°K , during this stage. Figures 3 and 4 show that the gas flow approaches the steady state. The steady state, shown in Figs. 5–7, is established at the time $t_{1\infty} = 200 \mu\text{s}$. Figure 5 shows gas density on the axis versus z , and Fig. 6 shows the two-dimensional gas density distribution in the vicinity of the supply channels and the gas velocity field lines. Figure 7 shows axial velocity distribution along the capillary axis. Figures 6 and 7 allow us to conclude that the gas is almost motionless in the capillary between the supply channels. The existence of such a steady-state gas flow is very important for the problem of the repetition rate. The expense of the gas in the steady state is equal to 0.14 mg/s per channel. The process of the relaxation towards the steady state together with the analogous results for stage 3 determine a recovery time for the steady-state gas density distribution.

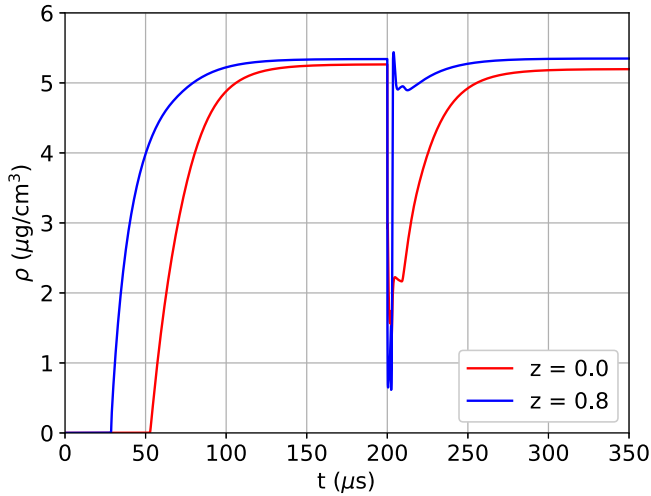


FIG. 4. The red line presents gas-plasma density evolution at the center of the capillary ($r = 0, z = 0$) during the all simulation: stages 1 + 2 + 3. The blue line shows the gas-plasma density evolution at $r = 0, |z| = 0.8$ cm, where the supply channels are.

When deviation of the gas density at $\rho(0, 0, t)$ from its steady state value, ρ_∞ , becomes less than 5%, temporal evolution of the gas density at $\rho(0, 0, t)$ is described by the expression

$$\rho(0, 0, t) \simeq \rho_\infty \left(1 - 0.5 \exp \frac{t_* - t}{\tau_{\text{sim}}} \right), \quad (2)$$

where $\rho_\infty = \rho(0, 0, t_{1\infty}) = 5.26 \mu\text{g}/\text{cm}^3$, $\tau_{\text{sim}} = 16.9 \mu\text{s}$, and $t_* = 66.7 \mu\text{s}$. Equation (2) gives reasonable approximation for simulated $\rho(0, 0, t)$ at the center of the capillary for time $t_{12} > t \gtrsim t_*$ (see Fig. 4). Below, in Sec. V A, we give a theoretical explanation of its exponential form.

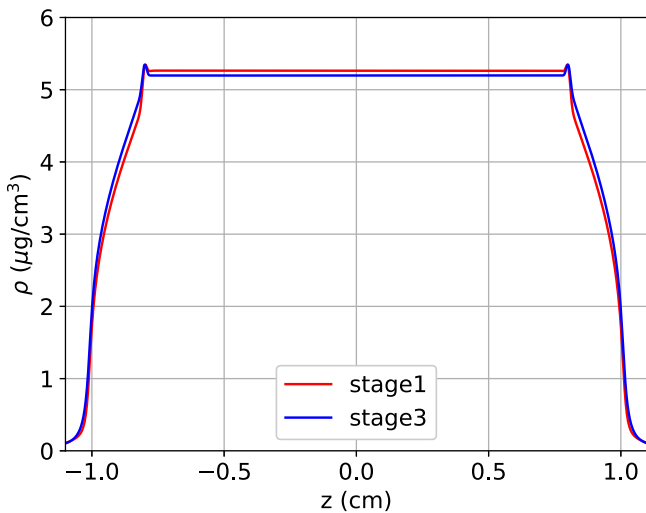


FIG. 5. Steady-state distributions of gas densities on the axis at asymptotically long times for stages 1 and 3.

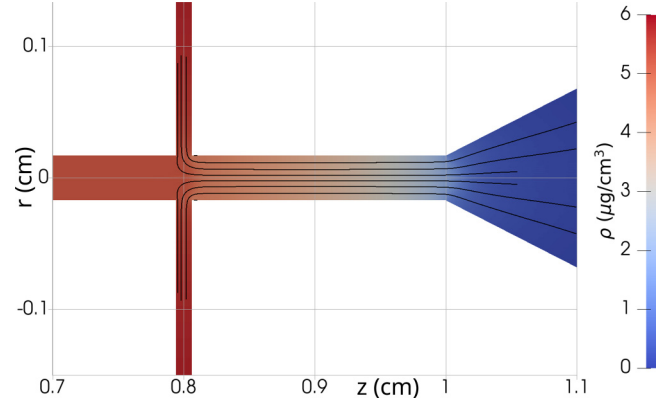


FIG. 6. 2D gas density distribution and lines of gas velocity at the steady state of stage 1. A spatial domain that is near the capillary end is shown only. In the region that is significantly to the left of the supply channel, the gas density is constant (see Fig. 5) and the gas is almost motionless (see Fig. 7).

B. Stage 2: Simulation of capillary discharge

We use the parameters of the steady-state gas flow, obtained in stage 1, as initial conditions for plasma dynamic simulation during the discharge stage. The considered model cannot describe the initial electric breakdown of the cold hydrogen gas. However, the breakdown lasts a short time, only about 10 ns, and presumably does not affect the plasma discharge properties considered in the present paper. Simulation of the second stage begins when gas becomes weakly ionized. Below, we consider results of the discharge simulation.

The present capillary discharge simulation differs in several important aspects from the 1D–3D simulations, whose results are presented in Refs. [31,45,46]. Transverse dynamics of the capillary plasma, leading to formation of the plasma channel suitable for laser pulse guiding, is similar to that considered in Ref. [31], where 1D approximation has been used. However, the 2D consideration shows that the lifetime of the short channel is determined by plasma outflow from the capillary ends, but not by the electric pulse duration as in the one-dimensional or long capillary cases (Ref. [46]).

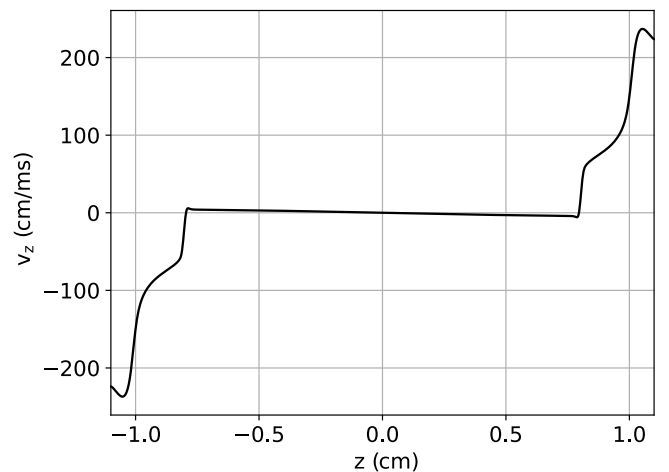


FIG. 7. Steady state velocity, $v_z(0, z, t_{1\infty})$, vs z for stage 1.

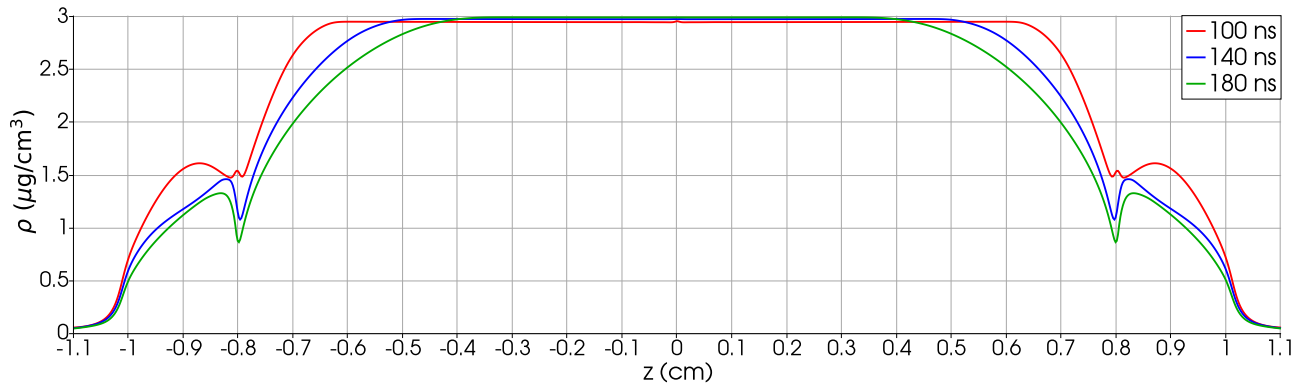


FIG. 8. Plasma density distributions during stage 2. We present results for the time interval, when well organized plasma channel of sufficient length exists. 1D plasma density distributions on the axis of the capillary are shown for different time moments. The curves are labeled by the time $t - t_{12}$. We see some depletions in the plasma density distributions at $|z| = 0.8$ cm. They correspond to the positions of the supply channels. See also Fig. 1. The ends of the capillary correspond to $|z| = 1$ cm.

Parameters of the present simulation are similar to the case considered in Ref. [45], where it was shown that the capillary length (1 cm) is too short to provide a sufficiently long axially homogeneous plasma channel. The plasma outflow into the supply channels shortened the effective length of axially uniform plasma channel. The latter effect was not taken into account in the 2D (r, z) -simulation [46] because the total capillary length was much larger than the distance between the supply channels and the capillary ends. The present capillary of 2 cm length is longer than the capillary considered in Ref. [45]; other parameters are similar, hence during a sufficiently long period, lasting about 80 ns, the length of axially homogeneous plasma channel is larger than 0.8 cm, as seen in Figs. 8–10. Figure 8 shows distribution of plasma density at $r = 0$ along the capillary axis for three time moments $t - t_{12} = 100, 140,$ and 180 ns. Figure 9 shows radial distribution of plasma density in the capillary center at $z = 0$ for the same time moments. We see the plasma

density minimum on the axis in the considered time interval. The plasma is completely ionized everywhere, excluding a thin layer of about $\sim 30 \mu\text{m}$ width near the capillary wall during the time interval $\sim 80 \text{ ns} < t - t_{12} < 300 \text{ ns}$. Figure 10 shows time dependence of ionization degree on the axis for different positions along the z axis. Electron density, n_e , is proportional to the plasma density at least for the part of the capillary channel ($|z| \leq 0.4$ cm) during the time interval $t - t_{12} = 100\text{--}180$ ns. Electron density on the axis is almost constant and approximately equal to $n_e = 1.8 \times 10^{18} \text{ cm}^{-3}$. The latter value fits the electron acceleration considered in Ref. [6]. For $0 < t - t_{12} < 180$ ns, transverse plasma dynamics in this part of the capillary is described by the 1D model [31]. Outside this region, plasma density distribution is affected by the plasma outflow of the open ends of the capillary and the gas supply channels. Two-dimensional distributions of the plasma parameters close to the orifices at $t - t_{12} = 140$ ns are shown in Figs. 11 and 12. They show that disturbances of the permanent gas flow in the supply channels do not propagate far from the capillary channel. At the time shown in

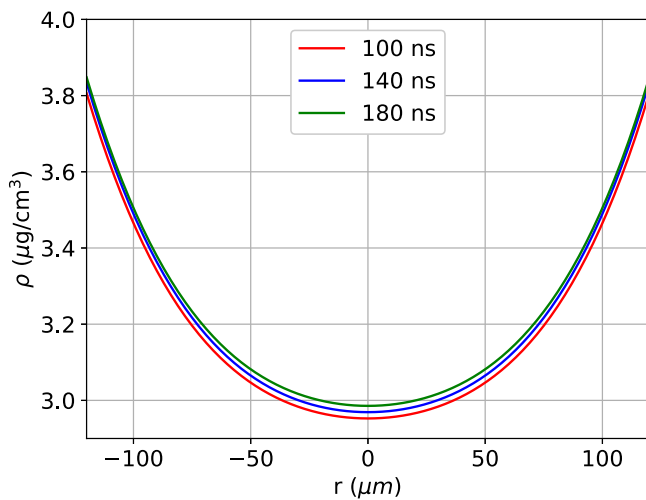


FIG. 9. Transverse plasma density distributions at $z = 0$ at the same time moments as in Fig. 8. The curves are labeled by the time $t - t_{12}$. The plasma is almost completely ionized at these moments (see Fig. 10). We note that these profiles represent also transverse electron density distributions.

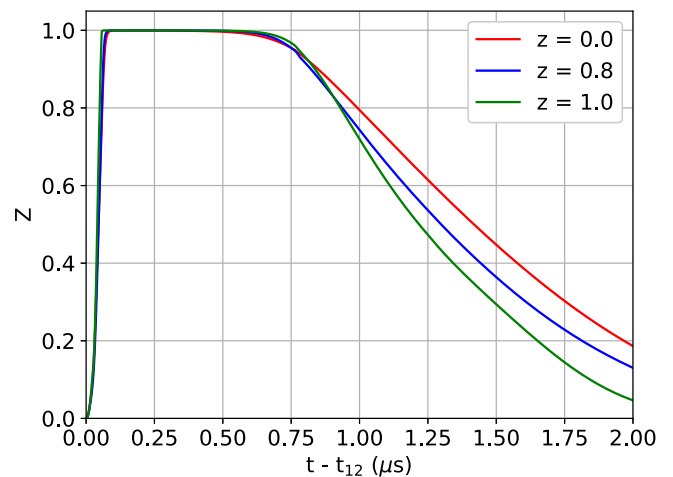


FIG. 10. Time dependencies of the mean ion charge Z on the axis for several positions along the axis during stage 2, labeled by z . Well-formed plasma channel for laser pulse guiding exists only while Z is of the order of 1.

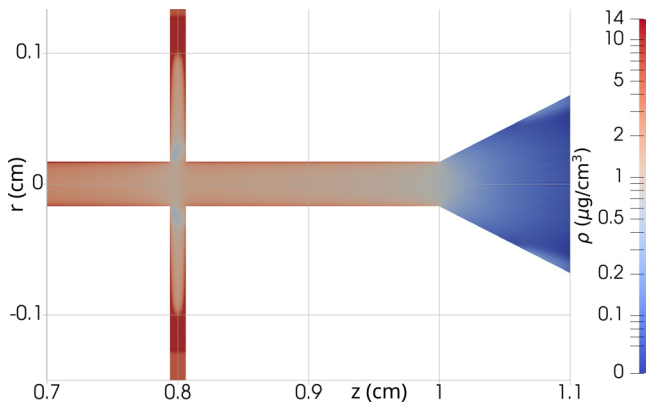


FIG. 11. Plasma density distribution in the vicinity of the orifice at $t - t_{12} = 140$ ns (stage2).

Figs. 11 and 12, the distance is of the order of 1–2 mm. This distance is about 3–4 mm in three-dimensional simulations in Ref. [45]. In any case, it is considerably less than the total length of the supply channels in the present simulations. Thus, we conclude that the simulated length of supply channels (1 cm) is sufficient for the simulation of the discharge recovering period for the considered capillary.

Figure 8 shows that plasma channels longer than 1 cm exist for a shorter time, $100 \text{ ns} < t - t_{12} < 140 \text{ ns}$.

The present simulation of the capillary discharge is extended till the moment of almost complete recombination of hydrogen. The further simulation of neutral gas behavior in the capillary till the next pulse of electric current is considered below in Sec. III C. High plasma pressure during the discharge and right after it leads to an outflow of almost all gas from the capillary. Figure 13 shows plasma density on the capillary axis versus time for several positions along the z axis ($|z| = 0, 0.8, \text{ and } 1 \text{ cm}$). The time dependencies of the axial density at the capillary ends and at the supply channel outlets, $|z| = 1$ and 0.8 cm , respectively, differ significantly from the time behavior of the axial plasma density in the main part of the capillary and, in particular, at the middle of the capillary, $z = 0$. Compare this time behavior with Fig. 8, where earlier moments are presented. This difference is caused by significant outflow of the plasma with considerably higher pressure than

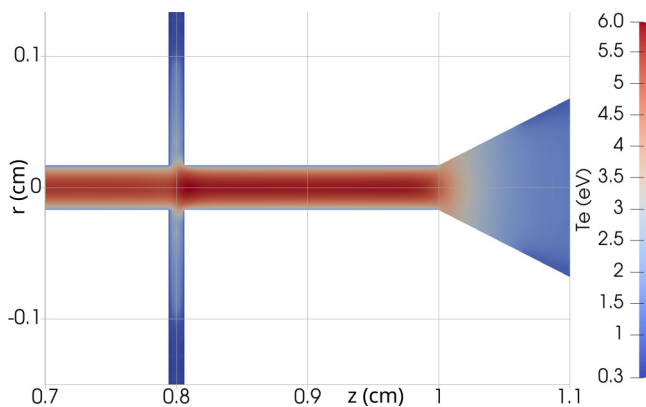


FIG. 12. Electron temperature distribution in the vicinity of the orifice at $t - t_{12} = 140$ ns (stage 2).

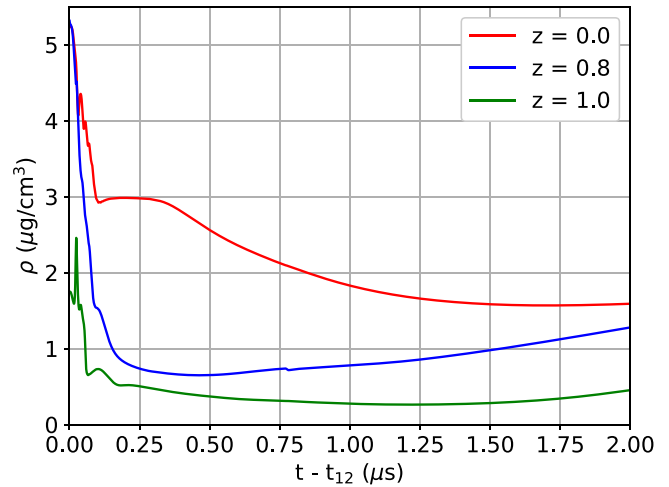


FIG. 13. Time dependencies of plasma density on the axis during stage 2 for several z .

the gas, initially filling the capillary and the channels, toward the open ends of the capillary, as well as toward the supply channels. The initial plasma density decrease on the axis occurs during the beginning of the discharge ($t < 80 \text{ ns}$) and corresponds to radial redistribution of the plasma density [31]. The redistribution leads to formation of the electron density radial profile (see Fig. 9), necessary for the laser guiding. The plasma temperature behavior during the discharge is shown in Fig. 14. Further plasma dynamics is determined mainly by plasma outflow from the capillary and by initial stage of its refilling. The gas-plasma pressure is diminishing due to the gas-plasma outflow and plasma cooling to the value, lower than the pressure inside the suppliers. The refilling starts approximately at $t - t_{12} \sim 500\text{--}700 \text{ ns}$ near the suppliers and at $\sim 1.25\text{--}1.5 \mu\text{s}$ at the middle of the capillary. The gas-plasma outflow is caused by plasma heating during the discharge. This process takes place in time interval $t_{12} = 200 \mu\text{s} < t < t_{23} = 202 \mu\text{s}$ (Fig. 4).

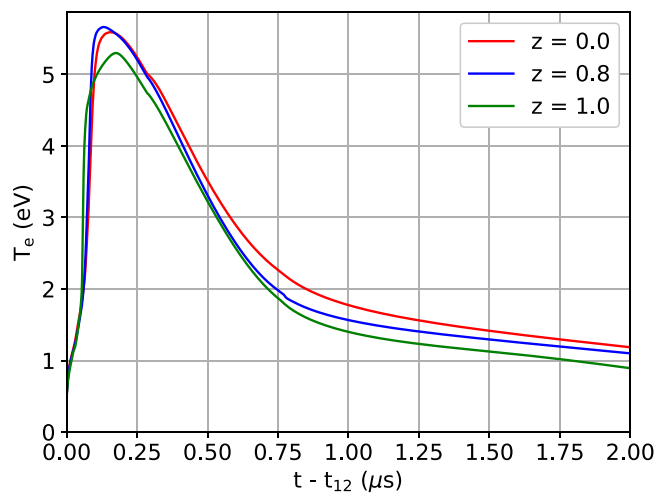


FIG. 14. Time dependencies of electron temperature on the axis during stage 2 for several values of z .

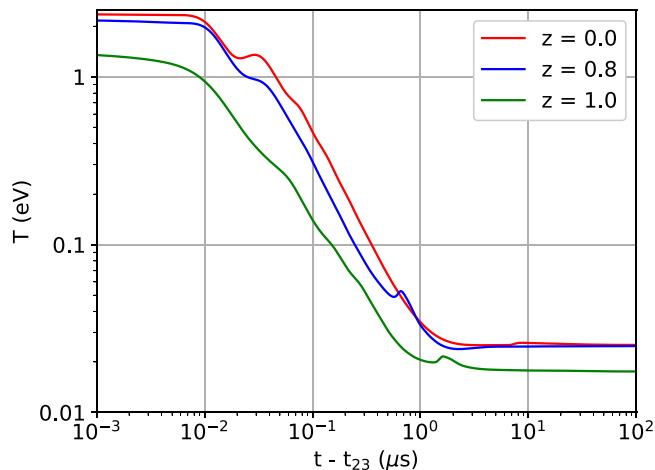


FIG. 15. Time dependencies of gas temperature on the axis during the beginning of stage 3 for several positions along the axis, labeled by values of z .

The plasma outflow is accompanied by the plasma cooling due to the thermal conduction to the cold capillary walls (see Fig. 14) and, hence, by the recombination (see Fig. 10). After the time $t - t_{12} = 2 \mu\text{s}$ the ionization degree becomes less than 0.2, and we end the simulation of stage 2.

C. Stage 3: Recovering of neutral gas distribution after the plasma discharge

We start stage 3 of simulation at the time $t = t_{23} = 202 \mu\text{s}$. The difference between stages 3 and 1 is as follows: (i) initial gas temperature in the capillary is considerably higher than the wall temperature (see Fig. 14); (ii) initial gas density is not zero, though is significantly lower than the steady state density at the first stage; and (iii) initially, the supply channels are not empty.

In the simulation of gas-plasma dynamics during stage 2, we use a plasma equation of state. This equation of state takes into account only atomic neutral particles. Simulating stage 3, we use equation of state, describing neutral molecular hydrogen, H_2 . These two different equations of states are not conjugated in the intermediate range of temperatures. So, we cannot exclude discontinuities at the time of the transition from stage 2 to stage 3. We set the gas-plasma density and pressure to be continuous functions of time at every spatial point. This approach provides absence of any mechanical shocks at the transition. Nevertheless, the gas temperature has a discontinuity at the transition time, t_{23} . However, this leads to a negligibly weak change in the gas flow parameters during a few microseconds after the beginning of stage 3. Figure 15 shows that the temperature relaxes on the timescale of a few microseconds to the capillary wall temperature. This relaxation time is considerably less than capillary refilling characteristic time ($100 \mu\text{s}$). As a result, such a temperature jump does not influence our main statements.

A similar problem occurs at the transition from stage 1 to stage 2. However, due to a very high rate of energy deposition during the electric breakdown of hydrogen at the onset of the electric current pulse, this period is very short and introduces much less inaccuracy into the simulation.

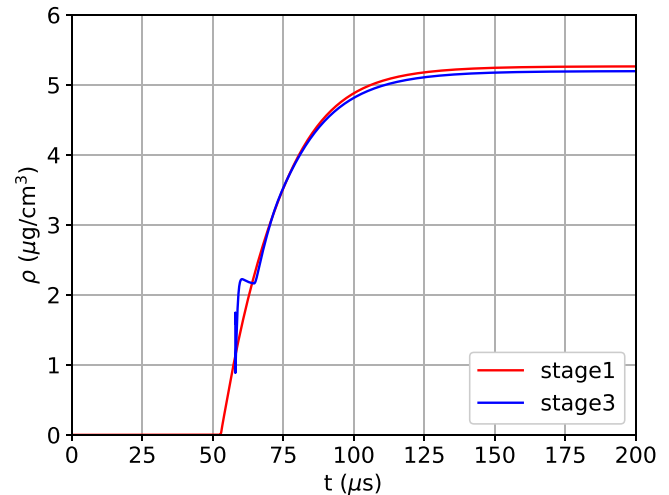


FIG. 16. Comparison of the gas density relaxation processes at the capillary center ($r = 0, z = 0$) for stages 1 and 3. The plot for stage 3 is shifted to the left by $144 \mu\text{s}$ for more clear comparison.

Stage 3 differs from stage 1 mainly in the initial conditions. In both stages, the initial gas densities are much smaller than steady-state ones. It is necessary to note that the initial gas densities in the supply channels are different. In stage 1, the initial gas density in the channels is equal to zero. In stage 3, it is of the order of the steady-state density except for the regions of the supply channels near the capillary. The geometry of the supply channels provides a small deviation of the initial density distribution in the supply channels right after the discharge from a steady-state distribution. The difference in the initial channel densities leads to delay of the filling process by $60 - 70 \mu\text{s}$ in stage 1 compared to stage 3 (see Fig. 4).

The initial gas temperatures are also different. It is approximately 2.2 eV in stage 3, and depends on r and z . Then gas temperature quickly relaxes to the wall temperature. Figure 15 shows that the relaxation process lasts about a few μs . The capillary refilling time is about $100 \mu\text{s}$. Comparing these times, we conclude that the higher initial temperature in stage 3 does not influence the recovering process.

Steady-state gas density distribution on the axis, obtained in the simulation at the end of stage 3, is shown in Fig. 5. We consider the distribution at $t = t_{3\infty} = t_{23} + 148 \mu\text{s}$ as a steady-state one. Relaxation of the central density, $\rho(0, 0, t)$ towards its steady-state value, ρ_∞ , is shown in Fig. 4 (see also Fig. 16 below). When deviation of the gas density, $\rho(0, 0, t)$, from its steady-state value, ρ_∞ becomes less than 5%, temporal evolution of the central gas density at is described by the following expression:

$$\rho(0, 0, t) \simeq \rho_\infty \left(1 - 0.5 \exp \frac{t_* - t}{\tau_{\text{sim}}} \right), \quad (3)$$

where $\rho_\infty = \rho(0, 0, t_{3\infty}) = 5.20 \mu\text{g}/\text{cm}^3$, $\tau_{\text{sim}} = 17.5 \mu\text{s}$, and $t_* = t_{23} + 8.0 \mu\text{s}$. Equation (3) gives reasonable approximation for simulated $\rho(0, 0, t)$ at the center of the capillary for time $t \gtrsim t_*$ (see Fig. 4). Below, in Sec. V A, we give a theoretical explanation of its exponential form. We note that the parameters ρ_∞ and τ_{sim} are almost the same for stages 1 and 3. This expression describes the relaxation of $\rho(0, 0, t)$

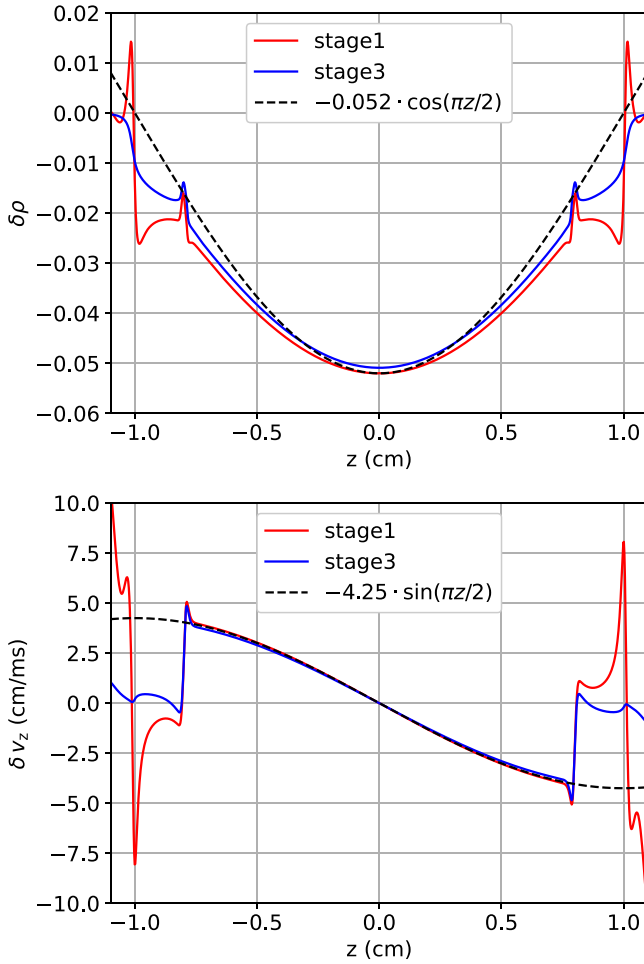


FIG. 17. Deviations of parameters of the gas flows from their steady-state values for stages 1 and 3 at the moments, when the relative deviations of the gas densities at the capillary center ($r = 0, z = 0$) are equal approximately to 0.05 of their steady-state values, $\rho(0, 0, t_\infty)$. The upper panel shows $\delta(z) = [\rho(0, z, t_{5\%}) - \rho(0, z, t = t_\infty)]/\rho(0, 0, t_\infty)$ for stages 1 and 3. The dashed line shows a fit of the form similar to the theoretical expression Eq. (7). The lower panel shows $\delta v_z(z) = v_z(0, z, t_{5\%}) - v_z(0, z, t_\infty)$ for stages 1 and 3. The dashed line shows the fit of the form Eq. (8). The theoretical fits in both panels are relevant only at $|z| < 0.8$ cm.

with a moderate accuracy up to times $t = t_*$, when the deviation from the steady-state value becomes about $0.5 \rho_\infty$. At $t - t_{23} > 100 \mu\text{s}$, the relative difference of the density distribution inside the capillary from the steady distribution becomes well below 1%. So, we estimate the neutral hydrogen distribution recovery time after the discharge for considered capillary parameters as $100 \mu\text{s}$. It corresponds to the 10 kHz repetition rate. The problem of the repetition rate will be considered in more detail below, in Sec. V.

D. Comparison of stages 1 and 3

Figure 16 shows relaxation of the gas density to steady state at the capillary center ($r = 0, z = 0$) for stages 1 and 3. To compare the plots, we shifted the third stage plot to the left by $144 \mu\text{s}$. We see that the plots approximately coincide. The difference is greater at the beginning of the stages, when

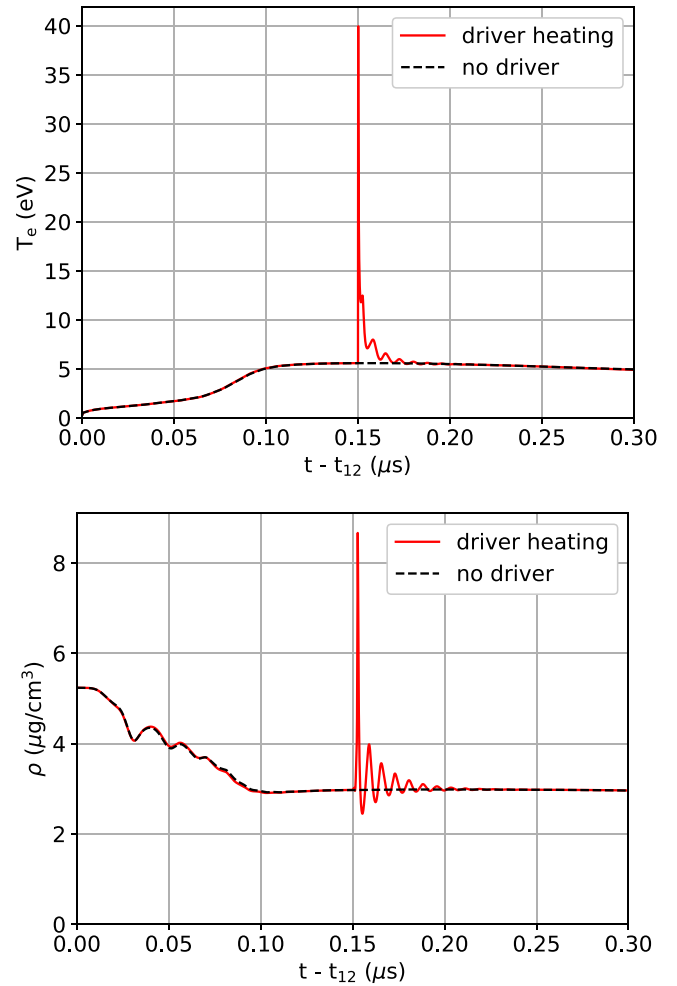


FIG. 18. Time evolution of the capillary plasma parameters after the driving laser pulse energy deposition. The upper panel shows electron temperature, the lower panel shows the plasma density at the capillary center ($r = 0, z = 0$). The solid lines correspond to the simulation with the laser pulse energy deposition, dashed lines to the simulation without the energy deposition.

the influence of the initial conditions is more important. The plots are approximated by Eqs. (2) and (3), when deviation of the gas density, $\rho(0, 0, t)$, from its steady-state value becomes less than 5%. It is necessary to note that simulations of the first and third stages result in almost the same values of τ_{sim} and ρ_∞ .

Thus, the relaxation to the steady-state flow develops in both stages in quite similar ways. Figure 17 shows the relative deviations of gas density and velocity along the axis from their steady-state values on the axis for both stages at the moment, when the relative deviations of the gas density and gas velocity along the capillary axis at the capillary center ($r = 0, z = 0$) from their steady-state values are 5%. We see that the distributions of gas density and velocity along the axis at the axis in both stages are similar.

We showed that the relaxation to the steady-state flow does not depend on a significant difference in the initial conditions. So, we can end the simulation of capillary discharge in the repetitive regime at the third stage because, if we continue

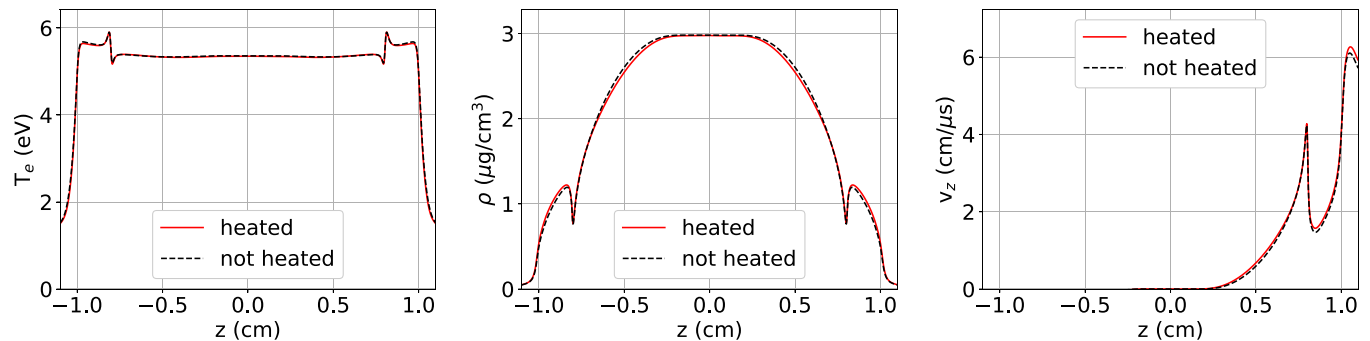


FIG. 19. Comparison of distributions of the electron temperature, T_e , (left panel) plasma density, ρ , (central panel) and plasma velocity, v_z , (right panel) along the capillary axis at the time $t = t_{12} + 230$ ns. The red and black dashed lines correspond to the versions with and without the laser pulse deposition, respectively.

to simulate the next discharge stage and then the recovering of the neutral gas distribution stage, we simply repeat the simulation of stages 2 and 3.

IV. EFFECT OF THE ENERGY DEPOSITION BY THE DRIVER LASER PULSE

The femtosecond laser pulse driving the wake wave deposit energy into the capillary plasma due to the generation of intense plasma wave and consequent thermalization of this energy into the internal energy of the electron component. The generation of the wake wave is a key point of the LWFA process, and its parameters are adjusted so the considerable part, ζ , of the laser pulse energy is spent for the plasma wave generation. Typically, this energy deposition is considerably larger than the energy deposited by the electric current pulse, creating the capillary plasma, and much higher than the current capillary plasma energy. It could be assumed that the dominating energy deposition leads to a considerable change of capillary plasma dynamics, however, it is not so. Below, we explain why we can neglect the effects from the femtosecond laser pulse.

To investigate the influence of the laser pulse energy deposition on the capillary plasma dynamics, we simulate pulsed energy deposition during the discharge (stage 2). The MHD code cannot simulate the plasma wave generation, damping, and energy transformation into plasma thermal energy. The duration of these processes (<0.1 ns) is much shorter than the duration of the electric current pulse (1). Then we consider that the hydrodynamic timescale duration of these processes is negligible. We set that an energy deposition takes place at $t = t_\ell$. At this moment of time, the electron temperature becomes $T_e = T_\ell$ in the vicinity of the axis, where $r \lesssim r_\ell$. The ion temperature, plasma densities, and velocities are not changed. Then we continue the simulation of stage 2.

We set for the present simulation: $t_\ell = t_{12} + 150$ ns, $T_\ell = 500$ eV, and $r_\ell = 100$ μm . These parameters correspond to $\zeta \simeq 3 \times 10^{-4}$ for the 3 J laser pulse.

Figure 18 shows time evolution of the electron temperature and plasma density at the capillary center, $r = 0$, $z = 0$, for the cases with and without the femtosecond laser pulse. We see that after approximately $t \sim 15$ – 20 ns after the laser pulse, the state of the capillary plasma returns back to the state without laser energy deposition. Nevertheless, small oscil-

lations in temperature and plasma density last for a longer time, about 30–50 ns after the laser pulse. Such behavior is determined by the plasma dynamics in the radial direction. For the considered capillary discharges, the characteristic time of this dynamics is much shorter than the electric current pulse characteristic time [31]. A similar problem is discussed in Refs. [18,36,38], where additional laser heating of capillary plasma is investigated to provide more pronounced guiding plasma channel.

The simulations show (see Fig. 19) that plasma parameters distributions at $t - t_{12} = 230$ ns remain almost the same as without the laser pulse. The difference between the simulations with and without laser pulse is negligible and we conclude that the laser energy deposition does not effect the recovery dynamics considered in Secs. III C and III D. The laser energy deposition leads to minor change of the overall capillary plasma dynamics. Figure 19 shows that at the time $t = t_{12} + 230$ ns, the contribution of the energy deposition to the plasma parameters is less than 2%. It leads to 0.5% variation in the recovering time.

In Fig. 18 (upper frame), we do not show the very short peak of electron temperature approximately equal to 500 eV and lasting about 0.03 ps in our hydrodynamic approximation after the almost instantaneous energy deposition from the driving laser pulse. This very short peak imitates in our simulations the energy deposition from the driving laser pulse as explained above in this section. During a short time after the energy deposition, when the ions can be considered as immobile, and the electron temperature is governed by thermal conduction, the electron temperature behaves as $T_e \propto (t - t_\ell)^{-2/5}$, and the typical temperature relaxation time is proportional to $T_e^{-5/2}$. This time becomes too short in the limit of large enough temperature to lead to any significant effect on the ion motion. Thus, the obtained results remain valid for any very short-time high-energy deposition. Hence, when $\zeta \gtrsim 10^{-4}$ the considered simulation gives a sufficiently accurate description of disturbed plasma dynamics at the timescales 1 – 20 ns.

V. CAPILLARY DISCHARGE PARAMETERS DETERMINING THE REPETITION RATE

In this section, we present a theoretical model giving the neutral gas density distribution recovering time and consider

the influence of the processes in the capillary plasma on the capillary wall heat balance. In this paper, we do not discuss the process of establishing the heat balance in the capillary walls [39]. Nevertheless, we consider here energy deposition from the capillary plasma to the wall.

A. Recovering time of the filling gas steady-state distribution in the capillary

The process of filling of the capillary with gas, shown in Figs. 4 and 16, does not possess oscillations. This can be a consequence of the significant role of viscosity in gas dynamics, and the gas flow can be considered a Poiseuille flow [49]. Then we consider the locally established Poiseuille flow [49] at each cross section of the capillary as a zero-order approximation, neglecting the role of the gas inertia. This yields the following expression for the total mass flow, q , through each cross section of the capillary [49]:

$$q = -k \frac{S^2 \rho}{\eta} \partial_z p = -k \frac{S^2 p}{\eta} \partial_z \rho. \quad (4)$$

Here S is the capillary cross section area, ρ is the gas density, η is the viscosity coefficient, and p is the gas pressure. According to the results, presented in Secs. III A, III C, and III D, we set the gas temperature equal to the capillary wall temperature. The gas pressure and density are constant across the cross section. The numerical coefficient, k , is of the order of unity. It depends on the form of the cross section. For the circular form cross-section capillary, the coefficient is $k = 1/8\pi \simeq 0.040$ [49]. We assume that the gas is ideal with constant heat capacity.

Using the mass conservation ($\partial_t S \rho + \partial_z q = 0$), we obtain the diffusion type equation for the gas density, ρ :

$$\partial_t \rho = k \partial_z \left(\frac{S p}{\eta} \partial_z \rho \right). \quad (5)$$

To estimate the relaxation time to the steady-state flow, we consider this equation in a close vicinity of the steady state: $\rho(z, t) = \rho_\infty + \rho_1(z, t)$, ($\rho_1 \ll \rho_\infty$). Here ρ_1 obeys the linear diffusion equation,

$$\partial_t \rho_1 = D \partial_z^2 \rho_1, \quad (6)$$

where the diffusion coefficient equals $D = k S p / \eta$. The latter linear equation has the lowest mode solution with the slowest relaxation rate:

$$\rho_1 = A \rho_\infty e^{-t/\tau} \cos \frac{\pi z}{L}, \quad (7)$$

$$v_z(r=0) = A \frac{\bar{k} L}{\pi^2 \tau} e^{-t/\tau} \sin \frac{\pi z}{L}. \quad (8)$$

Here $\bar{k} = 2$ for the circular cross section capillaries, L is the capillary length, and the relaxation time is

$$\tau = \frac{L^2}{\pi^2 D} = \frac{1}{k \pi^2} \frac{\eta L^2}{p S}. \quad (9)$$

The solution Eq. (7) satisfies the following boundary conditions at $|z| = L/2$: $p_1 = \rho_1 = 0$.

Equations (4) and (9) are obtained under the conditions

$$\tau \gg \frac{\rho r_0^2}{\eta}, \quad \tau \gg \frac{L}{c_s}. \quad (10)$$

Here, $c_s = \sqrt{p/\rho}$ is isothermal sound velocity of the gas.

For the parameters presented in Sec. II and the hydrogen viscosity coefficient (see Ref. [50]), the right sides of the inequalities Eqs. (10) are equal to 17 and 18 μs , respectively, whereas Eq. (9) gives $\tau \simeq 37.4 \mu\text{s}$. When the inequalities Eqs. (10) are not strong, the expression Eq. (9) is an estimation by the order of magnitude. The parameter, τ , obtained from simulation (see Secs. III A and III C) is approximately equal to $\tau_{\text{sim}} \simeq 17.4 \mu\text{s}$. The difference between τ and τ_{sim} indicates the accuracy of this estimation for the considered parameters [51]. For longer capillaries, the inequalities are stronger, then the expression Eq. (9) gives a more accurate estimation. Figure 17 shows simulated profiles ρ_1 and v_z for stages 1 and 3, when the amplitude of ρ_1 is about 5% ρ_∞ , and the solutions Eqs. (7) and (8) for ρ_1 and $v_z(r=0)$ at the same moment of time. $\rho_1 \approx A \rho_\infty \cos(\pi z/L)$, with $A = -0.05$. For v_z , we obtain $v_z \approx B \sin(\pi z/L)$, with

$$B = \frac{\bar{k} A L}{\pi \tau}. \quad (11)$$

For τ equal to the simulated value τ_{sim} , we find that $B \simeq 3.8 \times 10^3$ cm/s, whereas the fit in Fig. 17 corresponds to $B \simeq 4.4 \times 10^3$ cm/s. We see that there is reasonable accordance between the simple theory and simulation. It allows us to use the simple theoretical model for the estimations, especially for longer capillaries. The parts of the capillary between the supply channels and the open ends can influence the density distribution. The solution Eq. (7) neglects the length of these parts. As a result, an uncertainty in the estimation of the time, τ , caused by this simplification is less than 20% for considered parameters.

We calculated the parameters $k = 0.035$ and $\bar{k} = 2.1$ entering Eqs. (4), (5), (8), (9), and (11) for the square capillary [45,52].

If we rewrite the conditions Eqs. (10) in terms of the mean-free path of hydrogen molecules, λ_{aa} , both conditions become equivalent to each other and can be written in the form

$$\frac{L}{r_0} \gg \frac{r_0}{\lambda_{aa}}. \quad (12)$$

We note that the right-hand side of the inequality Eq. (12) very weakly depends on the gas temperature, which is approximately equal to the capillary wall temperature, but significantly depends on the gas density.

After time approximately equal to $\tau_0 \sim 10 \mu\text{s}$ after the discharge, the gas density distribution relaxes to a steady-state distribution. Let us compare this statement with Eq. (3). The value of $\rho(0, 0, \tau_0)$ is about half of its steady-state value. At time moment $\Delta t \simeq 4\tau + \tau_0$ after the discharge, the deviation of the gas density distribution from the steady-state distribution is of the order of 1%. It is possible to continue simulation of the capillary discharge in the repetitive regime with the period Δt repeating simulations of stages 2 and 3 in a loop. However, it is not necessary because the deviation of the obtained parameters from the steady state right before the onsets of the electric current pulse is of the order of 1% and does not possess any accumulating behavior because the geometry, gas supply pressure, and capillary wall temperature remain unchanged in accordance with our assumption.

We conclude that the repetition rate

$$f \simeq \frac{1}{C\tau + \tau_0}, \quad (13)$$

where $C = 4-5 \sim \ln 100$, is sufficient for complete recovery of neutral hydrogen distribution before the next current pulse. For the considered parameters, the repetition rate of 10 kHz is sufficient for the recovery. If the steady state temperature of the capillary wall is considerably higher than the room temperature, for example, equal to 1500 °K, then, according to Eq. (9), the recovery repetition rate is two times higher.

B. Energy deposition to the capillary wall

In the present paper, we do not consider in detail the problems of the heat balance in the capillary. We discuss only the contribution of the processes in plasma discharge and energy deposition by driver laser pulse to the heat balance in capillary walls. The repetition rate can be limited by the conditions, necessary to maintain the heat balance.

1. Energy deposition by the electric current

Capillary plasma is almost in thermal and mechanical equilibrium in the discharges of the type considered in Refs. [30,31,53]. The details are presented in Ref. [31]. We estimate the *mean* power, P , per unit capillary length deposited to the capillary wall [31] as

$$P[\text{W/cm}] = 85 \left(\frac{I_0[\text{kA}]}{r_0[\text{mm}]} \right)^{7/5} t_c[\mu\text{s}] f[\text{kHz}]. \quad (14)$$

Here, t_c is the time duration of the electric current pulse (FWHM) with the amplitude I_0 , and f is the discharge repetition rate. For the considered capillary discharge parameters. $P \sim 20$ W/cm for $f = 1$ kHz, whereas $P \sim 200$ W/cm for $f = 10$ kHz. The total power deposited in the 2-cm-length capillary is $W \sim 40$ and 400 W, respectively. To evaluate the importance of this effect, the latter values are compared with the results of the heat balance simulations in the capillary walls presented in Fig. 7 of Ref. [39].

We considered above the energy deposition rate averaged over the repetition period. However, the deposited power has narrow peaks during electric current pulses. They cause *pulsed* heating of a thin layer of the capillary wall in each cycle of the repetitive discharge. Such pulsed heating can damage the capillary after several cycles of the discharge operation. This problem was considered in Refs. [31,39,54]. Results obtained in Refs. [31,39,54] allow us to conclude that this pulsed effect can be neglected for the considered parameters of the capillary discharges.

2. Energy deposition by the driver laser pulse

Typical energy of the laser pulse, accelerating electrons to ~ 0.5 GeV, is estimated as 3 J [6]. We assume that a substantial portion, ζ , of this energy is deposited to the capillary plasma and is finally transferred to the plasma internal energy and then to the capillary wall. In Ref. [18], the coefficient ζ is approximately equal to 0.5. As a result, total *mean* power deposited to the capillary wall owing to this process equals $\zeta \times 3$ kW for $f = 1$ kHz and $\zeta \times 30$ kW for $f = 10$ kHz.

We discussed above that such energy deposition has a negligible effect on the recovery time of gas density distribution. Nevertheless, if we compare the latter values with the values presented above in Sec. VB 1, we see that the energy deposition by the driver laser pulse is higher than the capillary plasma energy contribution to the heat balance in the capillary.

If we compare the values presented in the previous paragraph with the results of simulations of heat balance in the capillary walls presented in Fig. 7 of Ref. [39], we conclude that laser energy deposited inside the capillary plasma leads to unacceptable heating of the capillary if the repetition rate is of the order of 10 kHz. This effect can be mitigated by the use of nitrogen cryogenic cooling [56] and/or capillaries made of diamond [39].

Let us consider the *pulsed* energy deposition in the capillary walls, caused by the driver laser pulse. The high peak temperature of the thin layer of the capillary wall after the laser pulse during ~ 100 ps can lead to melting or disintegration of the internal capillary wall. This effect is not directly related to the problem of the repetition rate. Nevertheless, it can limit the acceptable range of the driving laser pulse energies, capillary diameters, temperature regimes of the capillary, and its materials [18,33]. The capillary can withstand 10^6 [30] or 10^7 [39] shots without the driving laser pulse, depending on the capillary discharge parameters. A special experimental investigation of the capillary lifetime, when the driving laser was used [33], shows that an ablative plastic capillary withstands 140 shots. We assume that the nonablating sapphire capillaries, regularly used in many experimental works, demonstrate considerably longer lifetimes. Any detailed consideration of this important problem is beyond the scope of the present paper and demands a separate work.

VI. DISCUSSION AND CONCLUSIONS

The simulations of the capillary discharge in the repetitive regime show the following time-dependent gas-plasma dynamics. There is a permanent gas flow from the inlets of the supply channels to the vacuum region outside the ends of the capillary. The vacuum region is necessary for transportation of the driver laser pulses. This gas flow is disturbed by the electric current and driver laser pulse. Then the gas flow relaxes to its steady state for about 100 μs after the electric current pulse and the pulse of the driver laser. The gas flow is disturbed by the current and laser pulses and relaxes to the steady state between the pulses. The disturbances, caused by current and laser pulses, do not penetrate too far in the supply channels. Thus, the repetitive regime depends only slightly on the length of the simulated part of the supply channels if this length is sufficiently large.

Simulation of one cycle of repetitive operation of 2-cm-length and 0.34-mm-diameter capillary discharge shows that a plasma channel for laser pulse guiding of the length 0.8 cm and electron density on the axis about $2 \times 10^{18} \text{ cm}^{-3}$ exists for 80 ns, whereas the plasma channel of 1 cm length exists for shorter time, approximately equal to 40 ns. These conditions are favorable for high-quality electron beam generation with the energy of the order of 0.5 GeV [6]. For short capillaries the guiding plasma channel lifetime is determined by the plasma outflow from the open capillary ends and into the

supply channels. The electron density in the plasma channel is provided by the stationary hydrogen gas flow $\simeq 0.14$ mg/s per one supply channel. This requires electric current pulse of duration (FWHM) $\simeq 370$ ns with the amplitude of 200 A.

The simulation is split into three stages. The first stage models the process of the capillary filling with a molecular hydrogen gas before the discharge is ignited. The second stage models the capillary discharge till the cooling and recombination of the capillary plasma. The third stage models the recovery of the neutral hydrogen distribution after significant change during the previous stage. We show that a steady state of the gas flow is established at the end of the first and third stages due to permanent supply of hydrogen through the gas inlets. The steady state flow is established with an accuracy better than 1% after approximately 100 μ s after the electric current peak during the discharge stage. It means that we do not need to simulate further cycles of the capillary discharge operation in the repetitive regime if the capillary wall temperature, intensity of gas supply, and vacuum conditions outside the capillary remain unchanged. If the capillary wall temperature is of the order of the room temperature, the repetition rate can be 10 kHz. It provides complete recovering of the hydrogen gas density distributions between the consequent electric current pulses.

A significant part of the driver laser beam energy is deposited into the capillary plasma due to the plasma waves generation. This energy deposition is implemented in the simulation. We show that the deposited energy is larger than energy deposited into plasma by the electric current, but it causes negligible change in general gas-plasma dynamics. It happens because a characteristic time of transverse thermal equilibrium establishing is considerably shorter than duration of the electric current pulse for capillary discharges of considered type [31].

A simple model of relaxation to the steady state flow is developed in Sec. V A. The theoretical scaling for the relaxation time, τ , is given by Eq. (9). This model is compared with the simulations. The comparison shows that the simple model

gives reasonable recovery time for the parameters under consideration. For the parameters of the capillary discharge from the experiment [39], we obtain that the corresponding relaxation time, τ , is approximately 10 times longer than for considered here parameters. It corresponds to the repetition rate in Ref. [39], which was ten times less (1 kHz) than in the present paper. Our model shows that if the capillary wall temperature is considerably higher than the room temperature, then the recovering time of the neutral hydrogen gas is shorter than the time, obtained in our simulations. For larger capillary lengths the recovering time increases considerably in accordance with Eq. (9). It can be mitigated by adding extra supply channels between the two existing ones. The hydrogen gas pressure at the inlets of the channels should be less than the pressure for the existing channels to exclude gas flow in the capillary at the steady state.

We estimate the mean heat flux to the capillary wall from the capillary discharge caused both by the Joule heating of the capillary plasma and by the energy deposited by the driver laser pulses. Although energy deposition by the driver laser pulse leads only to a minor effect on the gas-plasma dynamics in the capillary and, hence, on the recovery time, nevertheless, this repeating energy deposition gives the main contribution to the heat flux to the capillary walls. Another important problem related to the energy depositions is damages of the capillary wall after a several cycles of the capillary discharge operation together with driving laser pulses [18,33]. This important problem is not related with the repetition rate and is out of the scope of the present paper.

ACKNOWLEDGMENTS

This research was funded by the project Advanced Research using High Intensity Laser produced Photons and Particles (ADONIS) (No. CZ.02.1.01/0.0/0.0/16_019/0000789) from European Regional Development Fund (ERDF) and by the Czech Technical University in Prague (No. RVO14000).

-
- [1] F. Grüner, S. Becker, U. Schramm, T. Eichner, M. Fuchs, R. Weingartner, D. Habs, J. Meyer-ter Vehn, M. Geissler, M. Ferrario, L. Serafini, B. van der Geer, H. Backe, W. Lauth, and S. Reiche, Design considerations for table-top, laser-based VUV and X-ray free electron lasers, *Appl. Phys. B* **86**, 431 (2007).
 - [2] M. Fuchs, R. Weingartner, A. Popp, Z. Major, S. Becker, J. Osterhoff, I. Cortrie, B. Zeitler, R. Hörlein, G. D. Tsakiris, U. Schramm, T. P. Rowlands-Rees, S. M. Hooker, D. Habs, F. Krausz, S. Karsch, and F. Grüner, Laser-driven soft-X-ray undulator source, *Nat. Phys.* **5**, 826 (2009).
 - [3] Z. Huang, Y. Ding, and C. B. Schroeder, Compact X-ray free-electron laser from a laser-plasma accelerator using a transverse-gradient undulator, *Phys. Rev. Lett.* **109**, 204801 (2012).
 - [4] M. E. Couprie, A. Loulergue, M. Labat, R. Lehe, and V. Malka, Towards a free electron laser based on laser plasma accelerators, *J. Phys. B* **47**, 234001 (2014).
 - [5] A. R. Maier, A. Meseck, S. Reiche, C. B. Schroeder, T. Seggebrock, and F. Grüner, Demonstration scheme for a laser-plasma-driven free-electron laser, *Phys. Rev. X* **2**, 031019 (2012).
 - [6] A. Molodzhentsev, G. Korn, A. Maier, and L. Pribyl, LWFA-driven free electron laser for ELI-beamlines, in *Proceedings of the 60th ICF Advanced Beam Dynamics Workshop (FLS'18), Shanghai, China, 5-9 March 2018, ICF Advanced Beam Dynamics Workshop No. 60 (JACoW, Geneva, 2018)*, pp. 62–67.
 - [7] R. W. Assmann, M. K. Weikum, T. Akhter, D. Alesini, A. S. Alexandrova, M. P. Anania, N. E. Andreev, I. Andriyash, M. Artioli, A. Aschikhin *et al.*, Eupraxia conceptual design report, *Eur. Phys. J.: Spec. Top.* **229**, 3675 (2020).
 - [8] K. Ta Phuoc, S. Corde, C. Thauray, V. Malka, A. Tafzi, J. P. Goddet, R. C. Shah, S. Sebban, and A. Rousse, All-optical Compton gamma-ray source, *Nat. Photon.* **6**, 308 (2012).
 - [9] C. G. R. Geddes, S. Rykovanov, N. H. Matlis, S. Steinke, J.-L. Vay, E. H. Esarey, B. Ludewigt, K. Nakamura, B. J.

- Quiter, C. B. Schroeder, C. Toth, and W. P. Leemans, Compact quasi-monoenergetic photon sources from laser-plasma accelerators for nuclear detection and characterization, *Nucl. Instrum. Methods. Phys. Res. B* **350**, 116 (2015).
- [10] K. Khrennikov, J. Wenz, A. Buck, J. Xu, M. Heigoldt, L. Veisz, and S. Karsch, Tunable all-optical quasimonochromatic Thomson X-ray source in the nonlinear regime, *Phys. Rev. Lett.* **114**, 195003 (2015).
- [11] W. Leemans and E. Esarey, Laser-driven plasma-wave electron accelerators, *Phys. Today* **62**(3), 44 (2009).
- [12] C. B. Schroeder, E. Esarey, C. G. R. Geddes, C. Benedetti, and W. P. Leemans, Physics considerations for laser-plasma linear colliders, *Phys. Rev. ST: Accel. Beams* **13**, 101301 (2010).
- [13] J. Faure, Y. Glinec, A. Pukhov, S. Kiselev, S. Gordienko, E. Lefebvre, J.-P. Rousseau, F. Burgy, and V. Malka, A laser-plasma accelerator producing monoenergetic electron beams, *Nature (London)* **431**, 541 (2004).
- [14] S. P. D. Mangles, C. D. Murphy, Z. Najmudin, A. G. R. Thomas, J. L. Collier, A. E. Dangor, E. J. Divall, P. S. Foster, J. G. Gallacher, C. J. Hooker, D. A. Jaroszynski, A. J. Langley, W. B. Mori, P. A. Norreys, F. S. Tsung, R. Viskup, B. R. Walton, and K. Krushelnick, Monoenergetic beams of relativistic electrons from intense laser-plasma interactions, *Nature (London)* **431**, 535 (2004).
- [15] J. Osterhoff, A. Popp, Z. Major, B. Marx, T. P. Rowlands-Rees, M. Fuchs, M. Geissler, R. Hörlein, B. Hidding, S. Becker, E. A. Peralta, U. Schramm, F. Grüner, D. Habs, F. Krausz, S. M. Hooker, and S. Karsch, Generation of stable, low-divergence electron beams by laser-wakefield acceleration in a steady-state-flow gas cell, *Phys. Rev. Lett.* **101**, 085002 (2008).
- [16] J. S. Liu, C. Q. Xia, W. T. Wang, H. Y. Lu, C. Wang, A. H. Deng, W. T. Li, H. Zhang, X. Y. Liang, Y. X. Leng, X. M. Lu, C. Wang, J. Z. Wang, K. Nakajima, R. X. Li, and Z. Z. Xu, All-optical cascaded laser wakefield accelerator using ionization-induced injection, *Phys. Rev. Lett.* **107**, 035001 (2011).
- [17] W. P. Leemans, A. J. Gonsalves, H.-S. Mao, K. Nakamura, C. Benedetti, C. B. Schroeder, C. Tóth, J. Daniels, D. E. Mittelberger, S. S. Bulanov, J.-L. Vay, C. G. R. Geddes, and E. Esarey, Multi-GeV electron beams from capillary-discharge-guided subpetawatt laser pulses in the self-trapping regime, *Phys. Rev. Lett.* **113**, 245002 (2014).
- [18] A. J. Gonsalves, K. Nakamura, J. Daniels, C. Benedetti, C. Pieronek, T. C. H. de Raadt, S. Steinke, J. H. Bin, S. S. Bulanov, J. van Tilborg, C. G. R. Geddes, C. B. Schroeder, Cs. Tóth, E. Esarey, K. Swanson, L. Fan-Chiang, G. Bagdasarov, N. Bobrova, V. Gasilov, G. Korn, P. Sasorov *et al.*, Petawatt laser guiding and electron beam acceleration to 8 GeV in a laser-heated capillary discharge waveguide, *Phys. Rev. Lett.* **122**, 084801 (2019).
- [19] T. Tajima and J. M. Dawson, Laser electron accelerator, *Phys. Rev. Lett.* **43**, 267 (1979).
- [20] E. Esarey, C. B. Schroeder, and W. P. Leemans, Physics of laser-driven plasma-based electron accelerators, *Rev. Mod. Phys.* **81**, 1229 (2009).
- [21] Igor I. Sobel'man, A. P. Shevelko, I. I. Sobelman, O. F. Yakushev, L. V. Knight, and R. S. Turleyb, A capillary discharge plasma source of intense VUV radiation, *Quantum Electron.* **33**, 3 (2003).
- [22] J. J. Rocca, V. Shlyaptsev, F. G. Tomasel, O. D. Gortazar, D. Hartshorn, J. L. A. Chilla, Demonstration of a discharge pumped table-top soft-X-ray laser, *Phys. Rev. Lett.* **73**, 2192 (1994).
- [23] B. R. Benware, C. D. Macchietto, C. H. Moreno, and J. J. Rocca, Demonstration of a high average power tabletop soft X-ray laser, *Phys. Rev. Lett.* **81**, 5804 (1998).
- [24] S. Karsch, J. Osterhoff, A. Popp, T. P. Rowlands-Rees, Z. Major, M. Fuchs, B. Marx, R. Hörlein, K. Schmid, L. Veisz, S. Becker, U. Schramm, B. Hidding, G. Pretzler, D. Habs, F. Grüner, F. Krausz, and S. M. Hooker, GeV-scale electron acceleration in a gas-filled capillary discharge waveguide, *New J. Phys.* **9**, 415 (2007).
- [25] W. K. H. Panofsky and W. R. Baker, A focusing device for the external 350-MeV proton beam of the 184-inch cyclotron at Berkeley, *Rev. Sci. Instrum.* **21**, 445 (1950).
- [26] J. van Tilborg, S. Steinke, C. G. R. Geddes, N. H. Matlis, B. H. Shaw, A. J. Gonsalves, J. V. Huijts, K. Nakamura, J. Daniels, C. B. Schroeder, C. Benedetti, E. Esarey, S. S. Bulanov, N. A. Bobrova, P. V. Sasorov, and W. P. Leemans, Active plasma lensing for relativistic laser-plasma-accelerated electron beams, *Phys. Rev. Lett.* **115**, 184802 (2015).
- [27] A. Butler, D. J. Spence, and S. M. Hooker, Guiding of high-intensity laser pulses with a hydrogen-filled capillary discharge waveguide, *Phys. Rev. Lett.* **89**, 185003 (2002).
- [28] D. J. Spence, A. Butler, and S. M. Hooker, Gas-filled capillary discharge waveguides, *J. Opt. Soc. Am. B* **20**, 138 (2003).
- [29] Y. Ehrlich, C. Cohen, A. Zigler, J. Krall, P. Sprangle, and E. Esarey, Guiding of high intensity laser pulses in straight and curved plasma channel experiments, *Phys. Rev. Lett.* **77**, 4186 (1996).
- [30] D. J. Spence and S. M. Hooker, Investigation of a hydrogen plasma waveguide, *Phys. Rev. E* **63**, 015401(R) (2000).
- [31] N. A. Bobrova, A. A. Esaulov, J.-I. Sakai, P. V. Sasorov, D. J. Spence, A. Butler, S. M. Hooker, S. V. Bulanov, Simulations of a hydrogen-filled capillary discharge waveguide, *Phys. Rev. E* **65**, 016407 (2001).
- [32] T. Hosokai, M. Kando, H. Dewa, H. Kotaki, S. Kondo, N. Hasegawa, K. Nakajima, and K. Horioka, Optical guidance of terrawatt laser pulses by the implosion phase of a fast Z-pinch discharge in a gas-filled capillary, *Opt. Lett.* **25**, 10 (2000).
- [33] T. Kameshima, H. Kotaki, M. Kando, I. Daito, K. Kawase, Y. Fukuda, L. M. Chen, T. Homma, S. Kondo, T. Z. Esirkepov, N. A. Bobrova, P. V. Sasorov, and S. V. Bulanov, Laser pulse guiding and electron acceleration in the ablative capillary discharge plasma, *Phys. Plasmas* **16**, 093101 (2009).
- [34] A. J. Gonsalves, K. Nakamura, C. Lin, D. Panasenkov, S. Shiraishi, T. Sokollik, C. Benedetti, C. B. Schroeder, C. G. R. Geddes, J. van Tilborg, J. Osterhoff, E. Esarey, C. Toth, and W. P. Leemans, Tunable laser plasma accelerator based on longitudinal density tailoring, *Nat. Phys.* **7**, 862 (2011).
- [35] A. Ferran Pousa, A. Martinez de la Ossa, R. Brinkmann, and R. W. Assmann, Compact multistage plasma-based accelerator design for correlated energy spread compensation, *Phys. Rev. Lett.* **123**, 054801 (2019).
- [36] C. Pieronek, A. Gonsalves, C. Benedetti, S. Bulanov, J. van Tilborg, J. Bin, K. Swanson, J. Daniels, G. Bagdasarov, N. Bobrova, V. Gasilov, G. Korn, P. Sasorov, C. Geddes, C. Schroeder, W. Leemans, and E. Esarey, Laser-heated capillary discharge waveguides as tunable structures for laser-plasma acceleration, *Phys. Plasmas* **27**, 093101 (2020).

- [37] N. A. Bobrova, P. V. Sasorov, C. Benedetti, S. S. Bulanov, C. G. R. Geddes, C. B. Schroeder, E. Esarey, and W. P. Leemans, Laser-heater assisted plasma channel formation in capillary discharge waveguides, *Phys. Plasmas* **20**, 020703 (2013).
- [38] G. A. Bagdasarov, N. A. Bobrova, O. G. Olkhovskaya, V. A. Gasilov, C. Benedetti, S. S. Bulanov, A. J. Gonsalves, C. V. Pieronek, J. van Tilborg, C. G. R. Geddes, C. B. Schroeder, P. V. Sasorov, S. V. Bulanov, G. Korn, and E. Esarey, Creation of axially uniform plasma channel in laser-assisted capillary discharge, *Phys. Plasmas* **28**, 053104 (2021).
- [39] A. J. Gonsalves, F. Liu, N. A. Bobrova, P. V. Sasorov, C. Pieronek, J. Daniels, S. Antipov, J. E. Butler, S. S. Bulanov, W. L. Waldron, D. E. Mittelberger, and W. P. Leemans, Demonstration of a high repetition rate capillary discharge waveguide, *J. Appl. Phys.* **119**, 033302 (2016).
- [40] A. Alejo, J. Cowley, A. Picksley, R. Walczak, and S. M. Hooker, Demonstration of kilohertz operation of hydrodynamic optical-field-ionized plasma channels, *Phys. Rev. Accel. Beams* **25**, 011301 (2022).
- [41] R. D'Arcy, J. Chappell, J. Beinortaite, S. Diederichs, G. Boyle, B. Foster, M. J. Garland, P. Gonzalez Caminal, C. A. Lindström, G. Loisch, S. Schreiber, S. Schröder, R. J. Shalloo, M. Thévenet, S. Wesch, M. Wing, and J. Osterhoff, Recovery time of a plasma-wakefield accelerator, *Nature (London)* **603**, 58 (2022).
- [42] B. Miao, J. E. Shrock, L. Feder, R. C. Hollinger, J. Morrison, R. Nedbailo, A. Picksley, H. Song, S. Wang, J. J. Rocca, and H. M. Milchberg, Multi-GeV electron bunches from an all-optical laser wakefield accelerator, *Phys. Rev. X* **12**, 031038 (2022).
- [43] V. Gasilov, A. Boldarev, S. Dyachenko, O. Olkhovskaya, E. Kartasheva, G. Bagdasarov, S. Boldyrev, I. Gasilova, V. Shmyrov, S. Tkachenko, J. Grunewald, and T. Maillard, Towards an application of high-performance computer systems to 3D simulations of high energy density plasmas in Z-Pinches, in *Applications, Tools and Techniques on the Road to Exascale Computing, Advances in Parallel Computing* Vol. 22 (IOS Press BV, Amsterdam, 2012), pp. 235–242.
- [44] O. G. Olkhovskaya, G. A. Bagdasarov, N. A. Bobrova, V. A. Gasilov, L. V. N. Goncalves, C. Lazzarini, M. Nevrkla, G. Grittani, S. S. Bulanov, A. G. Gonsalves, C. B. Schroeder, E. Esarey, P. V. Sasorov, S. V. Bulanov, and G. Korn, Plasma channel formation in the knife-like focus of laser beam, *J. Plasma Phys.* **86**, 905860307 (2020).
- [45] G. A. Bagdasarov, K. O. Kruchinin, A. Yu. Molodozhentsev, P. V. Sasorov, S. V. Bulanov, V. A. Gasilov, Discharge plasma formation in square capillary with gas supply channels, *Phys. Rev. Res.* **4**, 013063 (2022).
- [46] G. Bagdasarov, P. Sasorov, V. Gasilov, A. Boldarev, O. Olkhovskaya, C. Benedetti, S. Bulanov, A. Gonsalves, H. S. Mao, C. B. Schroeder, J. van Tilborg, E. Esarey, W. Leemans, T. Levato, D. Margarone, and G. Korn, Laser beam coupling with capillary discharge plasma for laser wakefield acceleration applications, *Phys. Plasmas* **24**, 083109 (2017).
- [47] E. V. Grabovski, V. V. Aleksandrov, G. S. Volkov, V. A. Gasilov, A. N. Gribov, A. N. Gritsuk, S. V. Dyachenko, V. I. Zaitsev, S. F. Medovshchikov, K. N. Mitrofanov, Ya. N. Laukhin, G. M. Oleinik, O. G. Olkhovskaya, A. A. Samokhin, P. V. Sasorov, and I. N. Frolov, Use of conical wire arrays for modeling three-dimensional MHD implosion effects, *Plasma Phys. Rep.* **34**, 815 (2008).
- [48] V. Aleksandrov, A. Branitski, V. Gasilov, E. Grabovskiy, A. Gritsuk, K. Mitrofanov, O. Olkhovskaya P. Sasorov, and I. Frolov, Study of interaction between plasma flows and the magnetic field at the implosion of nested wire arrays, *Plasma Phys. Control. Fusion* **61**, 035009 (2019).
- [49] L. D. Landau and E. M. Lifshitz, *Fluid Mechanics* (Oxford, Reed, 2000).
- [50] I. S. Grigoriev and E. Z. Meilikhov, *Handbook of Physical Quantities* (CRC Press, Boca Raton, FL, 1997).
- [51] Considering a damped oscillator ($\ddot{x} + 2\nu\dot{x} + \omega_0^2x = 0$), we have for the overdamped case: $\tau \approx 2\nu\omega_0^{-2}$, whereas for critical damping ($\nu = \omega_0$), we have $\tau = \omega_0$ that is two times longer than the overdamped limit predicts. This argument helps us understand that when both sides of the second strong inequality of Eq. (10) become of the same order, then we may be close to the critically damped regime and the parameter τ can be, in an extreme case, about two times less than the estimation Eq. (9), coming from the Poiseuille approximation, based on neglecting of gas inertia, gives.
- [52] G. Bagdasarov, P. Sasorov, A. Boldarev, O. Olkhovskaya, V. Gasilov, A. J. Gonsalves, S. Barber, S. S. Bulanov, C. B. Schroeder, J. van Tilborg, E. Esarey, W. P. Leemans, T. Levato, D. Margarone, G. Korn, and S. V. Bulanov, Plasma equilibrium inside various cross-section capillary discharges, *Phys. Plasmas* **24**, 053111 (2017).
- [53] P. Sasorov, Plasma dynamics in capillary discharges, in *X-Ray Lasers 2016: Proceedings of the 15th International Conference on X-ray Lasers*, Springer Proceedings in Physics, Vol. 202, edited by T. Kawachi, S. V. Bulanov, H. Daido, and Y. Kato (Springer, Cham, 2018), pp. 45–51.
- [54] M. Vrbova, P. Vrba, A. Jancarek, M. Nevrkla, N. A. Bobrova, and P. V. Sasorov, Wall ablation effect on the recombination pumping of EUV laser in pinching capillary discharge, *Phys. Plasmas* **26**, 083108 (2019).
- [55] E. M. Lifshitz and L. P. Pitaevskii, *Physical Kinetics* (Pergamon, New York, 1981).
- [56] Cooling of sufficiently pure and perfect crystal dielectrics leads to increasing of thermal conductivity coefficient [55] in the capillary wall and, hence, to decreasing the capillary internal wall temperature.